Electronic Supplementary Information

High Thermoelectric Performance in Sn-Substituted α-As_2Te_3

J. B. Vaney[1], J. Carreaud[2], G. Delaizir[2], A. Piarristeguy[3], A. Pradel[3], E. Alleno[4], J. Monnier[4], E. B. Lopes[5], A.P. Gonçalves[5], A. Dauscher[1], C. Candolfi[1], B. Lenoir[1*]

[1]*Institut Jean Lamour (IJL), UMR 7198 CNRS-Université de Lorraine, Nancy, France*

[2]*Sciences des Procédés Céramique et de Traitement de Surface (SPCTS), UMR CNRS 7315, Centre Européen de la Céramique, Limoges, France*

[3]*Institut Charles Gerhardt (ICG), UMR 5253 CNRS-Université de Montpellier, France*

[4]*Institut de Chimie et des Matériaux Paris Est (ICMPE), UMR 7182 CNRS-Université Paris-Est Créteil, Thiais, France*

[5]*C2TN, Instituto Superior Técnico, Universidade de Lisboa, Lisboa, Portugal*

[*]Corresponding author: bertrand.lenoir@univ-lorraine.fr

Contents

1. Rietveld refinements of the PXRD patterns of the *x* = 0.0, 0.025, 0.050 and 0.075 samples

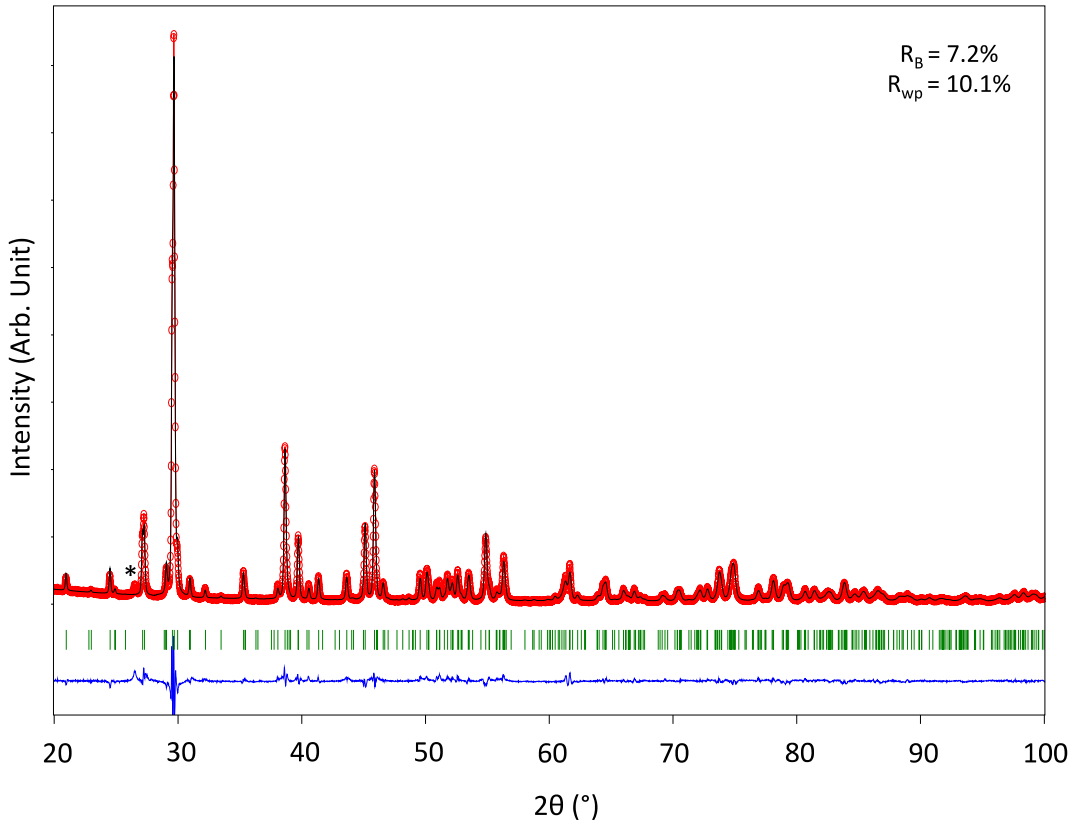

Figure S1. Rietveld refinement of the *x* = 0.0 sample. The open red circles are the experimental data, the black line is the calculated pattern, the bottom blue line is the difference between the experimental and calculated patterns and the green ticks correspond to the Bragg reflections. The asterisk marks the position of the reflection of the secondary phase attributed to AsTe.

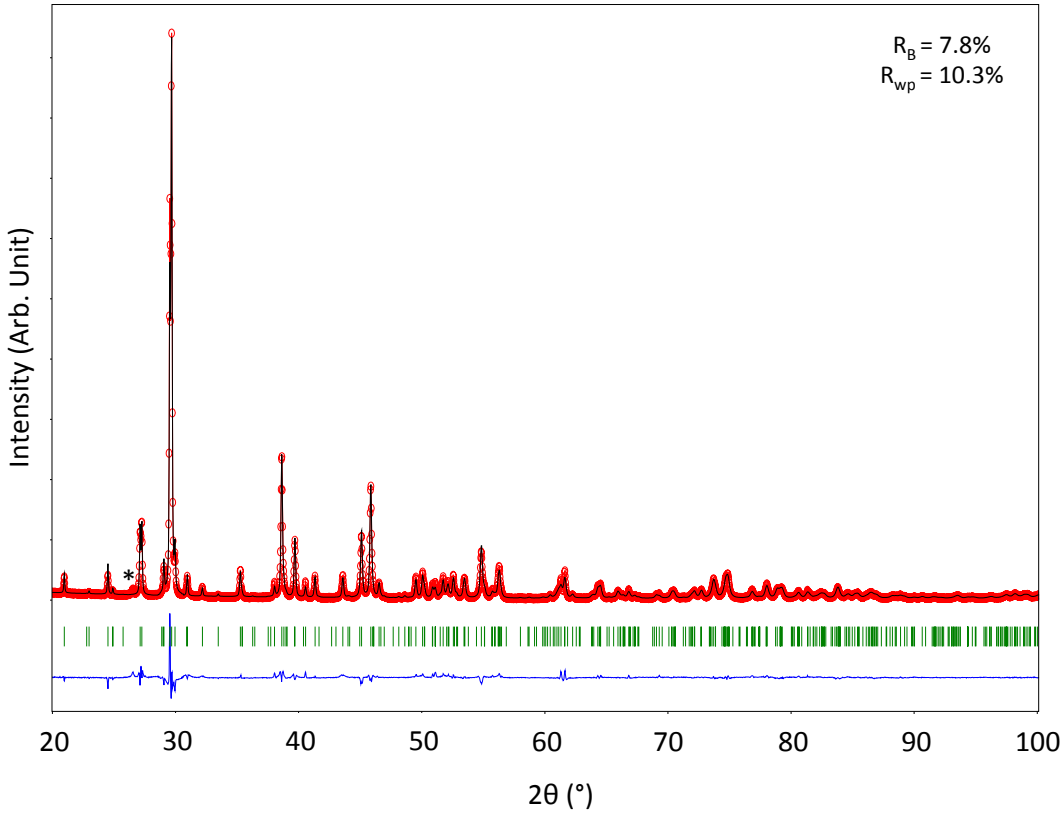

Figure S2. Rietveld refinement performed on the x = 0.025 sample. The weak additional reflection marked by an asterisk near ~26° corresponds to the cubic AsTe compound. Apart from this peak, all reflections can be indexed with the monoclinic space group C2/*m*.

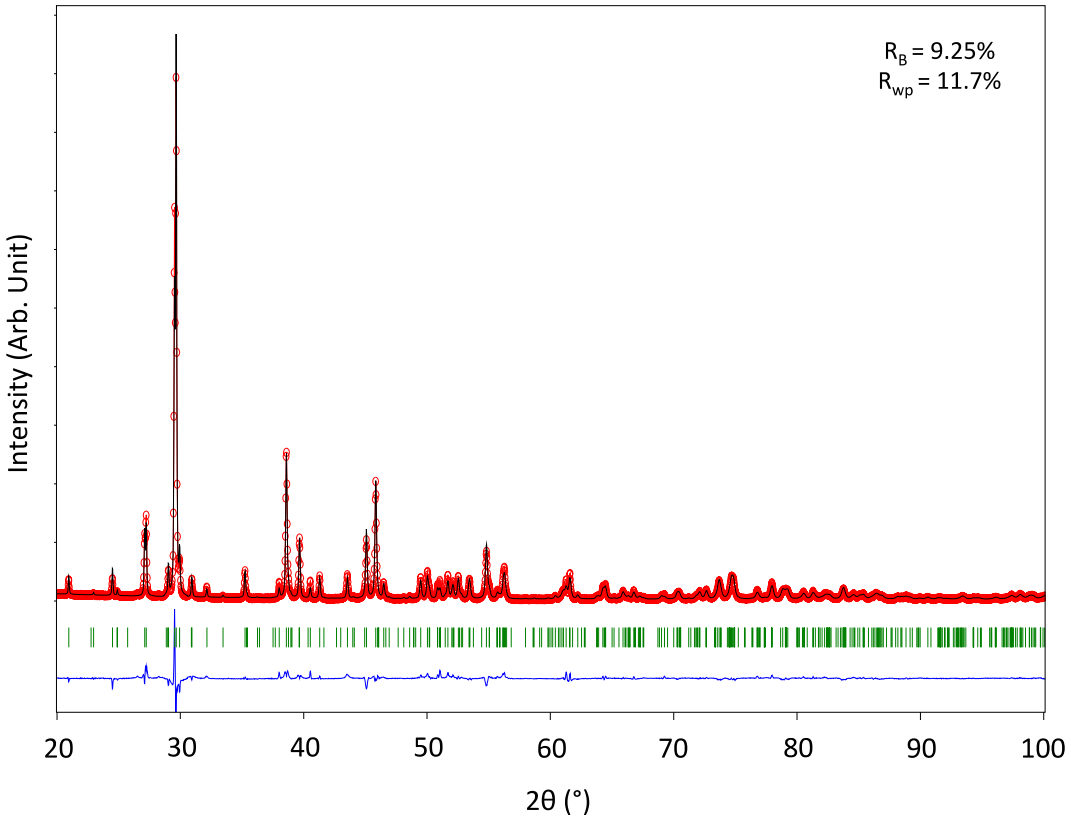

Figure S3. Rietveld refinement of the $x = 0.05$ sample.

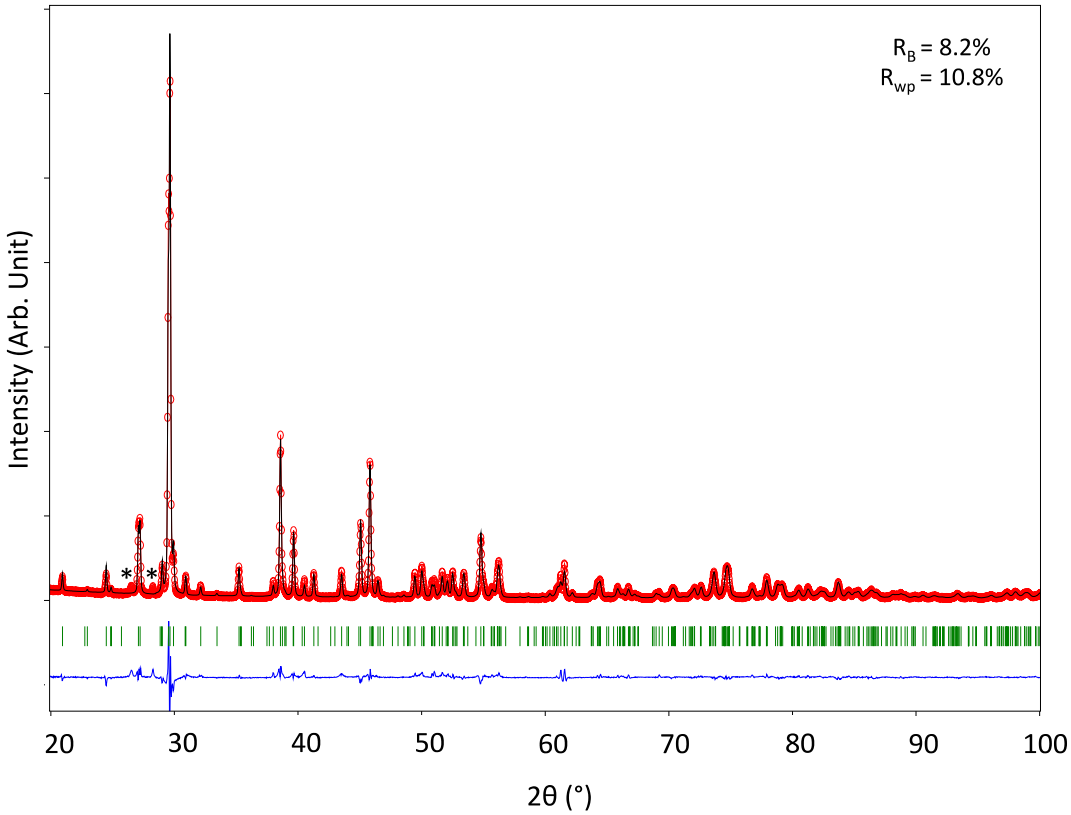

Figure S4. Rietveld refinement of the x = 0.075 sample. The asterisks correspond to the secondary phases identified as AsTe and elemental Te.

2. Backscattered electron images (BSE) and X-ray mapping of the α-$As_{2-x}Sn_xTe_3$ samples

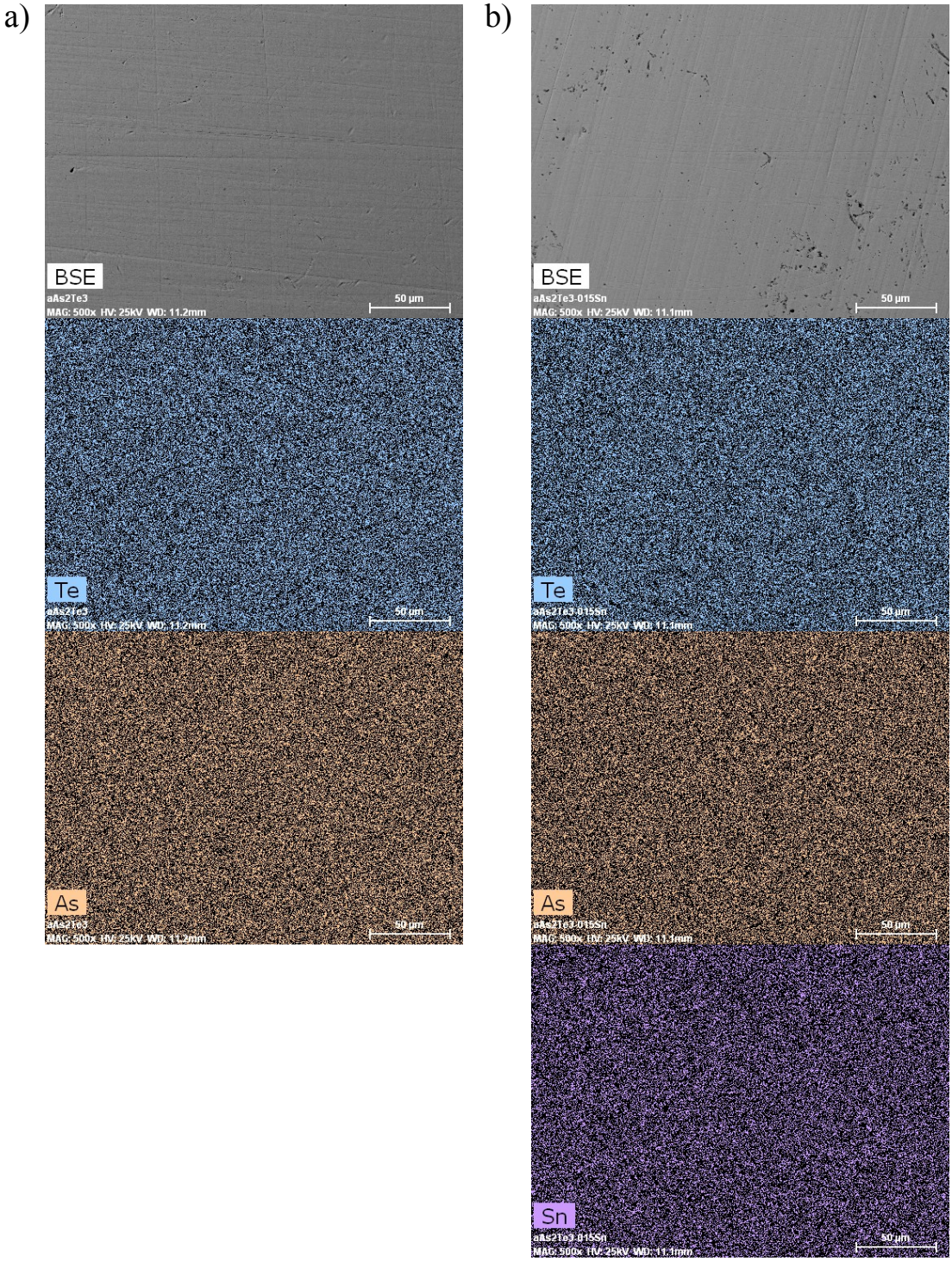

Figure S5. BSE images of the x = 0.0 (a) and 0.075 (b) samples.

3. DSC curve of α-As_2Te_3

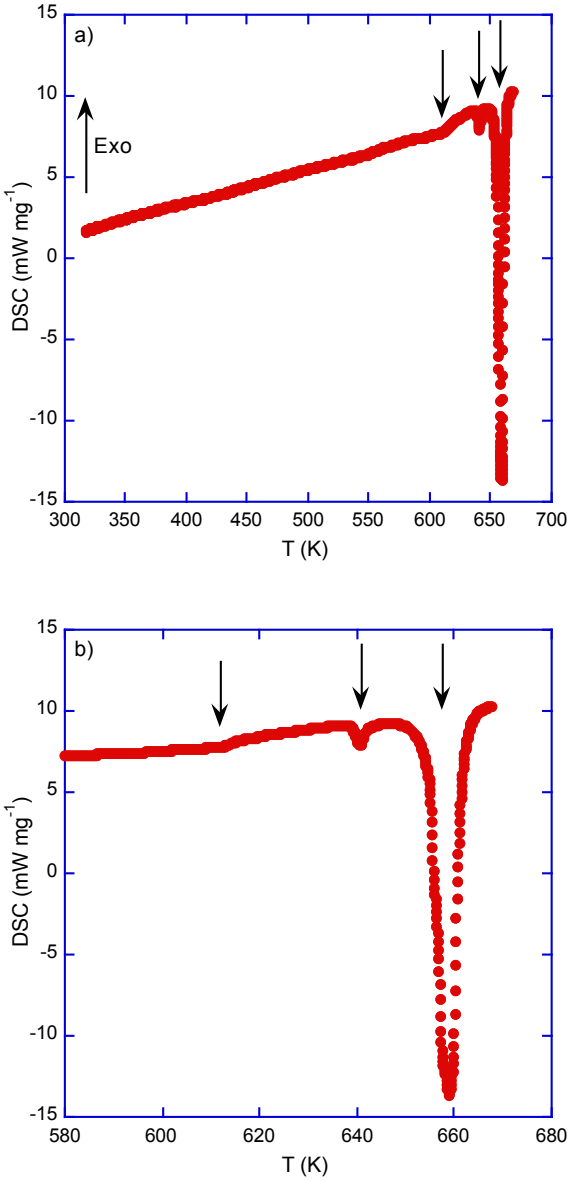

Figure S6. (a) DSC trace upon heating for α-As_2Te_3. (b) Magnification of the DSC trace around the three thermal events marked by the vertical arrows.

4. Electrical resistivity plotted as $\ln \rho$ versus T^{-1}

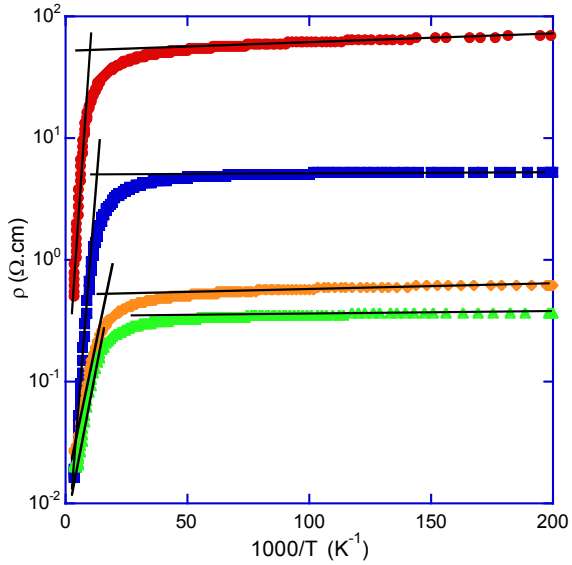

Figure S7. Log(ρ) versus inverse temperature for α-$As_{2-x}Sn_xTe_3$. The solid black lines indicate regions of activated temperature dependence.

5. High-temperature thermoelectric properties of a second specimen of α-As_2Te_3

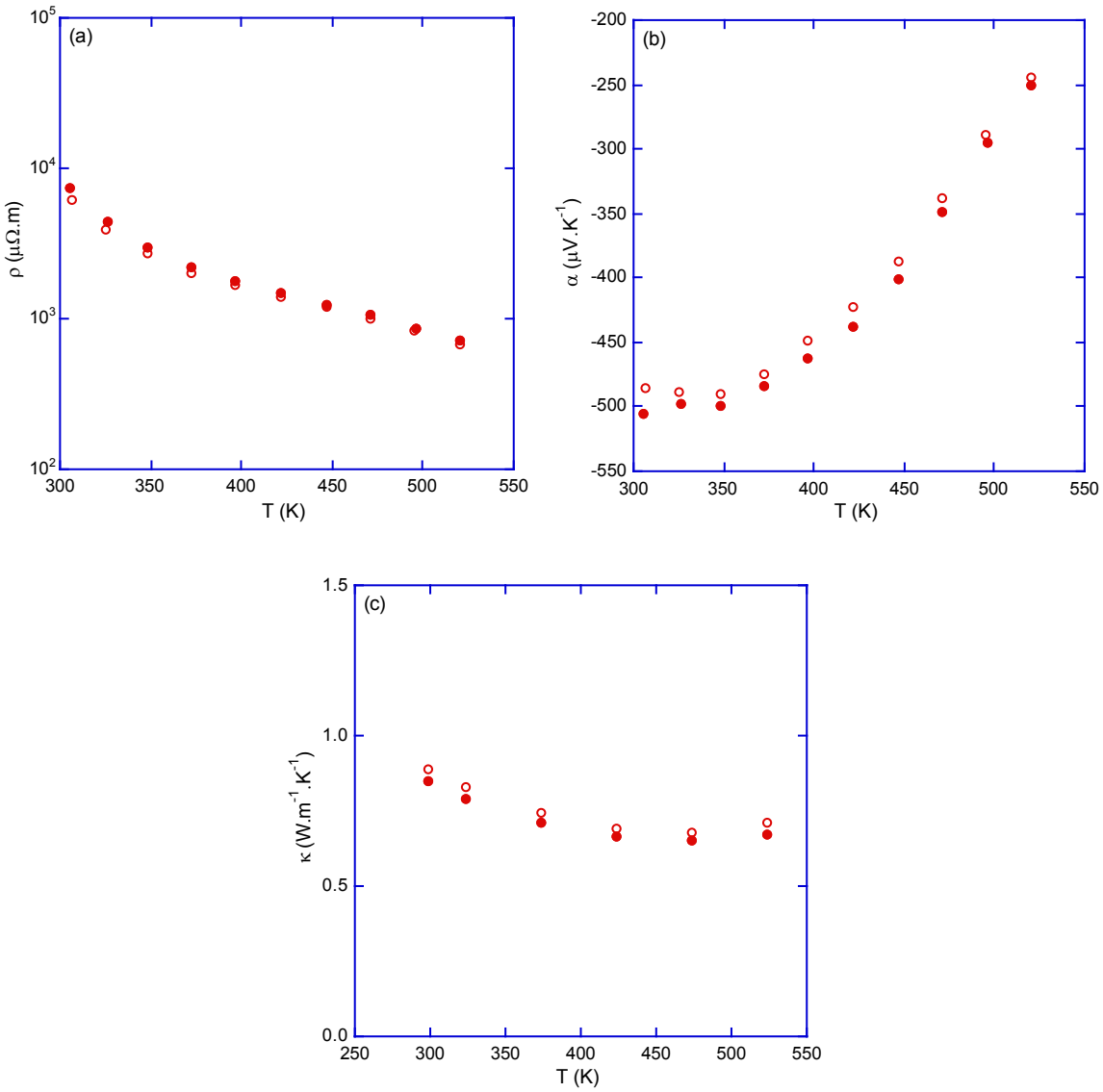

Figure S8. Temperature dependence of the electrical resistivity (a), thermopower (b) and total thermal conductivity (c) measured parallel (filled symbol) and perpendicular (open symbol) to the pressing direction in a second specimen of α-As_2Te_3 prepared under slightly different synthetic conditions. While the electrical resistivity is similar to that measured on the other sample, the thermopower shows large negative values indicating that this second sample is lightly *n*-type doped. The difference obtained between these two samples strongly suggests that

defects play a central role in determining the transport in this family as already widely studied in the Bi_2Te_3-based compounds. Further, the anisotropy seen in the thermopower data is strongly lessened compared to that observed in the other sample suggesting that the anisotropy is a function of the carrier concentration. If these defects have a marked influence on the electronic properties, the thermal transport remains practically unperturbed as shown by the thermal conductivity values that are nearly equivalent in both specimens.

6. Pisarenko plot of the α-$As_{2-x}Sn_xTe_3$ series

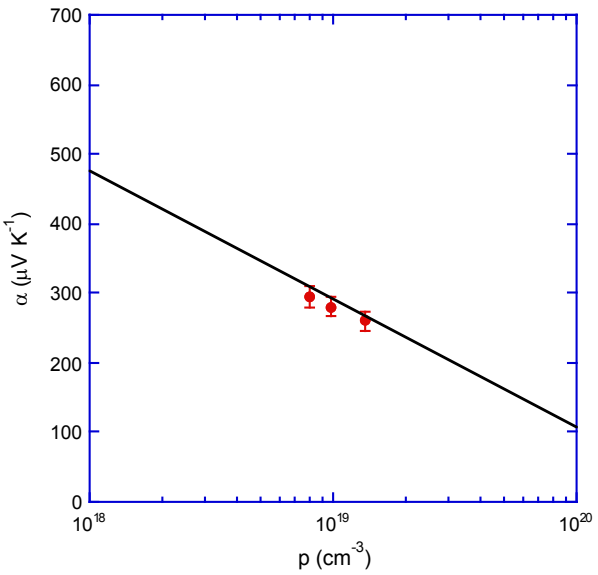

Figure S9. Hole concentration dependence of the thermopower at 400 K measured in the parallel direction. The experimental data are compared to the dependence predicted by the SPB model with an effective mass of 1.3 m_e (black solid curve).

7. Temperature dependence of the specific heat

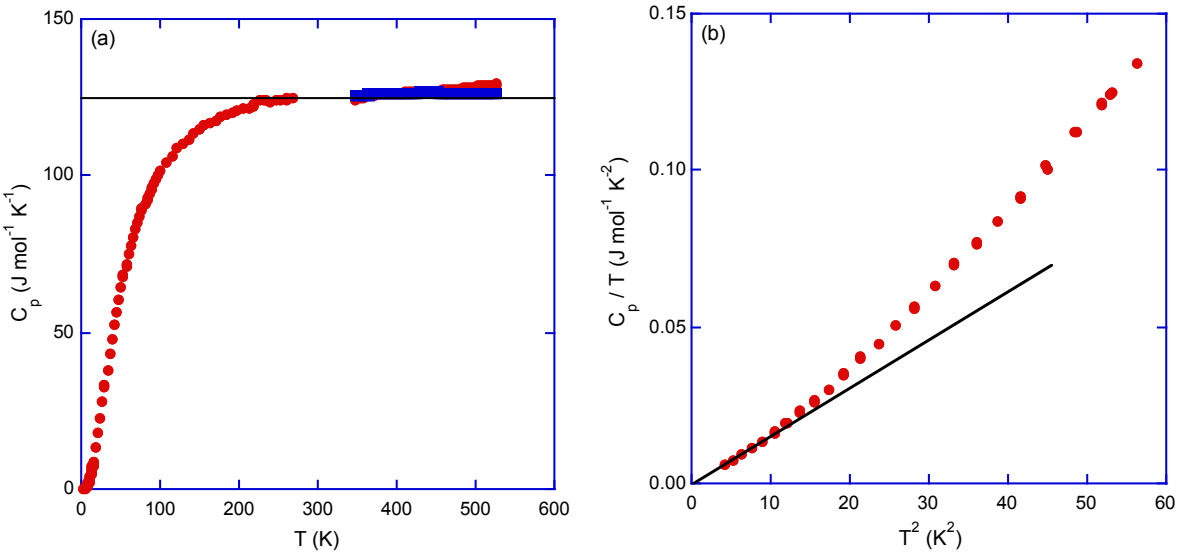

Figure S10. (a) Specific heat as a function of temperature of the x = 0.0 (red filled circles) and 0.05 (blue filled square) samples. The horizontal solid black line represents the Dulong-Petit value. The lack of data around 300 K is due to the addenda grease which gives an additional, extrinsic contribution to the specific heat. Near room temperature, the C_p values reach the Dulong-Petit limit that equals to $3NR$ where N is the number of atoms per formula limit and R is the gas constant. At high temperatures, the specific heat increases linearly with temperature above the Dulong-Petit value due to the thermal expansion of the unit cell. **(b)** Low-temperature specific heat data plotted as C_p / T versus T^2. The solid black line is a guide to the eye to underline the range where a linear behavior exists. The best fit to the data in this linear regime according to the free-electron formula $C_p / T = \gamma + \beta T^2$ yields a null Sommerfeld coefficient γ to within experimental uncertainty and a Debye temperature (related to the β parameter) of 179 K.

8. Crystallographic parameters of the α-$As_{2-x}Sn_xTe_3$ samples

Table S1. Crystallographic data of the α-$As_{2-x}Sn_xTe_3$ samples (space group C2/*m*, No. 12) derived from Rietveld refinements at 300 K. The lattice parameters *a*, *b* and *c* are given in Å, the angle β in ° and the volume *V* in $Å^3$.

x	0.0	0.025	0.050	0.075
a	14.3418(6)	14.3493(6)	14.3602(6)	14.3668(6)
b	4.0163(2)	4.0169(2)	4.0185(2)	4.0205(1)
c	9.8902(4)	9.8932(4)	9.8982(4)	9.9036(4)
β	95.060(2)	95.029(2)	95.001(2)	94.996(2)
V	567.47	568.07	569.01	569.88